J. Fluid Mech. (2012), *vol.* 708, *pp.* 397–417.
doi:10.1017/jfm.2012.316

Doubly symmetric finite-core heton equilibria

V. G. Makarov[1], M. A. Sokolovskiy[2] and Z. Kizner[3]†

[1] Interdisciplinary Center of Marine Sciences of the National Polytechnic Institute, La Paz, Baja California Sur 23096, Mexico

[2] Water Problems Institute of the Russian Academy of Sciences, 3 Gubkina Str. 119333, Moscow, Russia

[3] Departments of Physics and Mathematics, Bar-Ilan University, Ramat-Gan 52900, Israel

(Received 11 September 2011; revised 18 June 2012; accepted 20 June 2012; first published online 15 August 2012)

A finite-core heton is a baroclinic f-plane modon of a special type: it is composed of two patches of uniform quasi-geostrophic potential vorticity (PV) residing in different layers of a two-layer rotating fluid. This paper focuses on numerical construction of steadily translating, doubly symmetric, finite-core hetons and testing their stability. Such a heton, which possesses symmetry about the translation axis and the transverse axis, is a stationary solution to the equations of PV conservation in each of the layers when considered in a comoving frame of reference. When constructing the heton solutions and examining their bifurcations, we identify a heton by a pair of independent non-dimensional parameters, the half-length (in the translation direction) of a PV patch and the distance of the front point of the upper patch from the translation axis. The advantage of this method over other tried approaches is that it allows one to obtain solutions of new, previously unknown types. The results of testing the heton stability are presented on the plane made by a mean radius of a PV patch and the (horizontal) separation between the centroids of the patches. Two kinds of stability are tested separately, the stability to arbitrary perturbations that do not preserve the symmetry of the initial state and the stability to so-called symmetric perturbations that do not violate the initial symmetry. The hetons comparable in size with the Rossby radius, and smaller, are always stable in both senses. However, when some critical size is exceeded, the heton stability becomes dependent on the separation, and the larger the heton, the higher the separation required for stability. The separation guaranteeing the stability to symmetric perturbations is smaller than that required for the stability to arbitrary perturbations. Interrelations between instabilities and bifurcations are briefly discussed.

Key words: contour dynamics, rotating flows, vortex instability

1. Introduction

Theoretical study of quasi-geostrophic baroclinic vortical dipoles, or modons, dates back to 1980 when the first analytical two-layer solutions for steadily translating β-plane modons were reported (Flierl *et al.* 1980). During the past three decades, considerable progress has been made in developing the theory of baroclinic modons (Kizner 1984, 1997; Reznik & Sutyrin 2001; Kizner, Berson & Khvoles 2002, 2003*a*; Kizner *et al.* 2003*b*; Khvoles, McWilliams & Kizner 2007).

† Email address for correspondence: Ziv.Kizner@biu.ac.il

Whereas a translating barotropic vortical dipole (Lamb 1895; Chaplygin 1903; Larichev & Reznik 1976) can be viewed as a couple of interacting two-dimensional chunks of positive and negative vorticity located side by side, baroclinicity makes it possible for the two vortices of opposite sign to reside at different depths while having also some horizontal separation. The distributed baroclinic modon-with-a-rider solution (Flierl *et al.* 1980; Kizner 1984, 1997) represents just such a situation. Also a heton, a baroclinic configuration of two quasi-geostrophic point vortices of opposite signs confined to different layers of a rotating two-layer fluid and separated by a certain distance (Gryanik 1983; Hogg & Stommel 1985), falls in this category and thus can be thought of as a simplest finite-dimensional limit of the baroclinic modon solution.

Although a baroclinic modon and a point-vortex heton have the same mechanism of self-propulsion, the behaviour of a baroclinic modon can be much more complicated. This was demonstrated, for example, in numerical simulations with an analytical two-layer quasi-geostrophic modon solution categorized by continuity of its potential vorticity (PV) field. In addition to the smooth dipolar barotropic mode, such a modon bears a smooth circularly symmetric baroclinic mode (conventionally termed a rider). This solution, suggested originally for flows with continuous density stratification on the f- and β-planes (Kizner 1984, 1997), can be fitted to any two-layer stratification (Kizner *et al.* 2002, 2003*a*; see also Kizner 2008). The vorticity chunks constituting such a modon are confined in a circular separatrix and appear as separated both in depth and in the horizontal projection; when viewed from the top, they exhibit some overlap (see, e.g., Kizner 2008). In fact, a solution with a circular separatrix is a degenerate member of the family of solutions with non-circular separatrices (Kizner *et al.* 2003*a*). In particular, the magnitude of the baroclinic mode can be set arbitrarily in a circular-separatrix solution, which makes the degree of overlap a function of the ratio of the magnitudes of the baroclinic and barotropic modes; in addition, this ratio determines the stability or instability of this solution (Kizner *et al.* 2002). In contrast, in the semi-analytical solutions with elliptic separatrices (Kizner *et al.* 2003*a*), the overlap is determined by the aspect ratio of the ellipse. Two-layer numerical simulations (Kizner *et al.* 2002, 2003*a*; Khvoles *et al.* 2007) showed that the stability and evolution of circular- and elliptical-separatrix baroclinic modons strongly depend on the degree of overlap or, put another way, on the horizontal separation between the two vorticity patches, although this is not the only parameter on which the behaviour of a modon depends.

Determination of the key parameters affecting the stability of a baroclinic modon is the main motivation of our present study. In order to make progress in this line, a reasonable simplification of the concept of a baroclinic dipole is needed. In this respect, the point-vortex heton is too simple a model, because such a heton is unconditionally stable. More appropriate for the declared aim appears the concept of a finite-core heton, a two-layer quasi-geostrophic vortical structure composed of two oppositely signed patches of uniform PV residing in different layers (Sokolovskiy 1988; Polvani 1991; Sokolovskiy & Verron 2000). The term ‘finite-core heton’ was suggested by Polvani (1991), who constructed the first steady-state solutions of this kind. We emphasize the fact that a finite-core heton is a particular case of a baroclinic modon, namely, a two-layer modon with a stepwise PV distribution in each layer.

The subject of our interest in this paper is translating finite-core f-plane doubly symmetric hetons. The double symmetry of a heton means that the layer thicknesses are equal, and the shapes of the two PV patches arranging a heton possess symmetry

about the translation axis (for definiteness, this will be the x-axis) and about the transverse axis as well. The PV in the two patches of a symmetric heton is assumed constant, opposite in sign and equal in absolute value (so, strictly speaking, such hetons should be called antisymmetric). Note that neither of the above-listed conditions is necessary for the existence of a stationary solution for a translating heton (see, e.g., § 2.3). These constraints, however, limit the number of free parameters determining a heton to two, thus making the search for the hetons feasible

To obtain a heton solution, an iterative procedure (which fits into the concept of contour dynamics) will be used, based on the fact that, in a frame of reference comoving with the heton, the contours bounding the PV patches are stationary. Earlier, some doubly symmetric hetons were obtained by Polvani (1991).

We shall construct a two-parameter family of doubly symmetric hetons, choosing for the identification of a heton its half-length γ^* (in the translation direction) relative to the Rossby radius and the non-dimensional distance h from the front point of its upper-layer PV patch to the translation axis. The properties of the hetons found will be discussed both using the parameters γ^* and h, and in terms of the mean radius γ of a PV patch (again relative to the Rossby radius) and the non-dimensional horizontal separation d between the centroids of the patches.

First, classification of the doubly symmetric heton equilibria will be carried out on the (γ^*, h) and (γ, d) planes and their bifurcations will be examined in detail. Next, the stability of the hetons will be tested with contour-dynamics simulations, in which the numerical noise will serve as a perturbing factor. We shall formulate qualitative and quantitative stability criteria and examine separately the stability to arbitrary (asymmetric) perturbations that do not preserve the symmetry of the initial state, and the stability to antisymmetric perturbations, i.e. to perturbations that do not violate the initial symmetry; for brevity, the perturbations of the latter type will be referred to as symmetric. The results of testing the heton stability will be presented on the plane (γ, d) and supplemented by a brief discussion of the interrelation between instabilities and bifurcations.

The two-layer quasi-geostrophic model, the two-layer contour dynamics, and the method for capturing the doubly symmetric heton equilibria are described in § 2. The two-parameter family of such hetons, its limiting states and bifurcations are presented and discussed in § 3 and the stability issue is discussed in § 4.

2. Model and methods

2.1. *Two-layer quasi-geostrophic model*

A quasi-geostrophic flow in a two-layer inviscid incompressible rotating fluid is described by the equations of PV conservation, where the characteristics of the flow in each layer are functions of the horizontal coordinates x and y only. Assuming the unperturbed thickness H of each of the two layers to be the same and the Coriolis parameter f constant (the f-plane model), these equations can be written in a non-dimensional form as follows:

$$\partial q_1/\partial t + J(\psi_1, q_1) = 0, \quad \partial q_2/\partial t + J(\psi_2, q_2) = 0, \tag{2.1}$$

$$q_1 = \Delta\psi_1 - \tfrac{1}{2}\gamma^2(\psi_1 - \psi_2), \quad q_2 = \Delta\psi_2 + \tfrac{1}{2}\gamma^2(\psi_1 - \psi_2). \tag{2.2}$$

Here q_1, q_2, ψ_1 and ψ_2, are the potential vorticities and streamfunctions in layers 1 and 2, which, for definiteness, will be referred to as the upper and the lower layer, respectively; Δ and J are the Laplacian and Jacobian in x, y. The streamfunction ψ_i in layer i is related to the x and y components of the flow velocity, u_i and v_i, via the

equations

$$u_i = -\partial\psi_i/\partial y, \quad v_i = \partial\psi_i/\partial x, \quad i = 1, 2. \tag{2.3}$$

Parameter $\gamma = L/L_{Ro}$ in (2.2) is the ratio of the length scale L of the flow to the Rossby deformation radius $L_{Ro} = \sqrt{gH\delta\rho/(2f^2\rho)}$, where g is the acceleration due to gravity, and ρ and $\delta\rho$ are the mean density and the density jump between the layers. If L is fixed, then γ is a characteristic of the density stratification. On the other hand, when constructing a heton solution, for the purposes of classification of the solutions found, it is profitable to fix the stratification (i.e. L_{Ro}) and regard L as a characteristic size of the heton. Accordingly, in such a case, the non-dimensional size of any heton becomes 1, and γ becomes the heton's size relative to the Rossby radius. The heton's dimensional size L can be defined in different ways. By setting $L = \sqrt{S/\pi}$ with S being the area of one PV patch, we choose the patch mean radius as the heton's size (Kozlov, Makarov & Sokolovskiy 1986; Polvani 1991). An alternative definition will be introduced in § 2.3. As the time scale in the contour-dynamics simulations, we use $1/\bar{q}$, where $\bar{q}$ is the mean (over the patches) absolute value of PV.

A convenient commonly used representation of a two-layer flow is its decomposition into the barotropic and baroclinic components, $\psi_1 = \psi_{BT} + \psi_{BC}$, $\psi_2 = \psi_{BT} - \psi_{BC}$, $q_1 = q_{BT} + q_{BC}$ and $q_2 = q_{BT} - q_{BC}$ or, equivalently,

$$\psi_{BT} = \tfrac{1}{2}(\psi_1 + \psi_2), \quad \psi_{BC} = \tfrac{1}{2}(\psi_1 - \psi_2), \quad q_{BT} = \tfrac{1}{2}(q_1 + q_2), \quad q_{BC} = \tfrac{1}{2}(q_1 - q_2). \tag{2.4}$$

Thus, the barotropic and baroclinic potential vorticities are given by the Laplace and Helmholtz operators,

$$q_{BT} = \Delta\psi_{BT}, \quad q_{BC} = \Delta\psi_{BC} - \gamma^2\psi_{BC}. \tag{2.5}$$

This decomposition is used below, where the two-layer contour-dynamics algorithm is briefly presented (§ 2.2). It is also helpful in understanding the structure of some limiting heton solutions (§ 3.2).

2.2. *Two-layer contour dynamics*

The contour dynamics method was suggested by Zabusky, Hughes & Roberts (1979) for two-dimensional Euler vortical flows. It was later generalized to incorporate the contour surgery that enables reconnection of vorticity contours (Dritschel 1988) and to make the method applicable to two-layer and continuously stratified quasi-geostrophic flows (Kozlov *et al.* 1986; Helfrich & Send 1988; Polvani, Zabusky & Flierl 1988; Dritschel 1989).

Although a heton, the subject of this study, is a pair of simply connected patches of uniform PV of which one resides in layer 1 and the other in layer 2, the contour surgery may lead to splitting of a PV patch into several disconnected parts. This situation can be handled by considering several contours in the same layer. (In principle, this approach covers also the case of non-simply connected domains; however, we skip the details of this issue as it is beyond the scope of our present paper.) The numbers N_1 and N_2 of contours bounding simply connected domains of uniform PV patches emerging in layers 1 and 2 may be different and can change over time. Therefore, when describing the computational algorithm we will use the subscript $i = 1, 2$ and the bracketed superscript $j = 1, \ldots, N_i$ to identify contour j in layer i, and will denote the PV jump across this contour in the direction of its inward normal as $q_i^{(j)} = \text{constant}$. (In a contour-dynamics simulation initialized by a symmetric heton, $q_i^{(j)} = \pm 1$.)

Following Kozlov *et al.* (1986), we parametrize the boundary contour of a specific patch by a parameter λ that varies continuously in some range $0 \leqslant \lambda \leqslant \Lambda$. Accordingly, the coordinates $\xi_i^{(j)}$ and $\eta_i^{(j)}$ of a point on the boundary contour of patch j residing in layer i become periodic functions of λ; to indicate also the dependence of $\xi_i^{(j)}$ and $\eta_i^{(j)}$ on time, we shall write $\xi_i^{(j)} = \xi_i^{(j)}(\lambda, t)$ and $\eta_i^{(j)} = \eta_i^{(j)}(\lambda, t)$. Using such a parameterization, the velocity components of the flow induced by the ensemble of N_1 upper-layer and N_2 lower-layer PV patches are calculated as

$$u_1(x, y, t) = a_1 + \tfrac{1}{2}(c_1 - c_2), \quad u_2(x, y, t) = a_2 - \tfrac{1}{2}(c_1 - c_2), \tag{2.6}$$

$$v_1(x, y, t) = b_1 + \tfrac{1}{2}(d_1 - d_2), \quad v_2(x, y, t) = b_2 - \tfrac{1}{2}(d_1 - d_2), \tag{2.7}$$

where

$$\left.\begin{aligned} a_i &= \frac{1}{2\pi}\sum_{j=1}^{N_i} q_i^{(j)} \int_0^{\Lambda} [\eta_i^{(j)}(\lambda, t) - y] g_i^{(j)}(\lambda, x, y, t)\, \mathrm{d}\lambda, \\ b_i &= -\frac{1}{2\pi}\sum_{j=1}^{N_i} q_i^{(j)} \int_0^{\Lambda} [\xi_i^{(j)}(\lambda, t) - x] g_i^{(j)}(\lambda, x, y, t)\, \mathrm{d}\lambda, \end{aligned}\right\} \tag{2.8}$$

$$\left.\begin{aligned} c_i &= \frac{1}{2\pi}\sum_{j=1}^{N_i} q_i^{(j)} \int_0^{\Lambda} [K_0(\gamma R_i^{(j)}) + \ln(R_i^{(j)})] \dot{\xi}_i^{(j)}\, \mathrm{d}\lambda, \\ d_i &= \frac{1}{2\pi}\sum_{j=1}^{N_i} q_i^{(j)} \int_0^{\Lambda} [K_0(\gamma R_i^{(j)}) + \ln(R_i^{(j)})] \dot{\eta}_i^{(j)}\, \mathrm{d}\lambda. \end{aligned}\right\} \tag{2.9}$$

In (2.9), K_0 is the zero-order modified Bessel function; dot denotes differentiation with respect to λ; the function $g_i^{(j)}$ appearing in (2.8) is defined by the formula

$$g_i^{(j)}(\lambda, x, y, t) = \frac{1}{(R_i^{(j)})^2}\{\dot{\eta}_i^{(j)}[\xi_i^{(j)}(\lambda, t) - x] - \dot{\xi}_i^{(j)}[\eta_i^{(j)}(\lambda, t) - y]\}, \tag{2.10}$$

where $R_i^{(j)}$ is the distance between a point (x, y) and a point $(\xi_i^{(j)}, \eta_i^{(j)})$ on the edge of patch j in layer i,

$$R_i^{(j)} = \sqrt{[\xi_i^{(j)}(\lambda, t) - x]^2 + [\eta_i^{(j)}(\lambda, t) - y]^2}. \tag{2.11}$$

In the derivation of formulae (2.6)–(2.9), the decomposition of the flow into a sum of the barotropic and baroclinic flows is employed. So the functions ln and $-K_0$, which are Green's functions of the Laplace and Helmholtz operators, respectively, represent here the barotropic flow and the baroclinic flow (see (2.5)). In the particular case, where the flows in the two layers are identical, the baroclinic component vanishes, and formulae (2.6)–(2.11) can be simplified (cf. formulae (2.9)–(2.10) of Makarov & Kizner (2011)).

The velocity at which a point $(\xi_i^{(j)}, \eta_i^{(j)})$ on a boundary contour moves is calculated via (2.6) and (2.7) (with the use of (2.8)–(2.11)), where $\xi_i^{(j)}$ and $\eta_i^{(j)}$ are substituted for x and y,

$$\frac{\mathrm{d}\xi_i^{(j)}}{\mathrm{d}t} = u_i(\xi_i^{(j)}, \eta_i^{(j)}, t), \quad \frac{\mathrm{d}\eta_i^{(j)}}{\mathrm{d}t} = v_i(\xi_i^{(j)}, \eta_i^{(j)}, t). \tag{2.12}$$

Once the boundary contours are discretized by distributing a set of nodes over each contour at a distance ΔC, relationships (2.12) become a finite set of first-

order ordinary differential equations. These equations are solved with a fourth-order Runge–Kutta method; time is discretized with a step Δt, running over a given interval $0 \leqslant t \leqslant T$, while the integrals in (2.8) and (2.9) are computed with the use of a periodic cubic spline. The cubic spline is also used for the uniform redistribution of the nodes over each contour at every time step. The contour surgery (when need) is carried out using an original code of Makarov (1991).

Along with the stability to (generally) asymmetric perturbations, a particular case is considered, where the perturbations do not violate the antisymmetry of the upper- and lower-layer flows about the x-axis, inherent in the unperturbed state. For this purpose we use a modified version of the contour-dynamics code, in which this symmetry is preserved (this approach was earlier applied by Polvani (1991)). The characteristic feature of this version is that, at any time step, only the coordinates of the boundary contours in the upper layer are computed via (2.12). The shapes of the boundary contours in the lower layer are obtained as mirror images (with respect to the x-axis) of those in the upper layer; the upper-layer velocity field, however, is calculated as induced by the PV patches in both layers. This version of the algorithm is referred below to as mirror-symmetric.

In the contour-dynamics simulations, parameter γ is varied in a wide range, whereas the initial areas of the vorticity patches are taken equal to π. Such unification allows us to use fixed time and length (along a contour) steps Δt and ΔC, respectively, for all simulations. For testing the heton stability, we apply $\Delta t = 0.05$ and $\Delta C = 0.02$ (the latter corresponds to 314 nodes over a circle of unit radius) and, normally, run the simulations up to $T = 1000$–5000. However, even when a run lasted up to $T = 30\,000$ the changes in the area of an individual patch of a stable heton never exceeded 0.05 %.

2.3. *Capturing the shapes of stationary hetons*

The key ideas of contour dynamics are advantageous also when relative equilibria of finite-area vortices, or V-states, are sought for; the first achievements in this line were due to Deem & Zabusky (1978) and Wu, Overman & Zabusky (1984). A relative equilibrium is an ensemble of vortices that can move as a whole, translationally or rotationally, at either a constant linear or angular velocity, but keeps unchanged the shapes and mutual arrangement of the vortices. A relative equilibrium, therefore, is a stationary state when considered in a comoving frame of reference. Capturing of such a heton is based on the fact that, in a comoving frame of reference, the total velocity in any point of a contour bounding a vorticity patch should be tangent to the contour. This (relative) velocity is a difference of the velocity in a fixed frame of reference and the translation speed of the heton. Putting it differently, the stationarity condition consists in vanishing of the scalar product of two vectors, the velocity of a particle located at a boundary contour of a PV patch, and a normal (to the contour) vector at this point. At this stage, since a stationary heton comprises only one uniform-vorticity patch in each layer, the superscript (j) can be omitted and one may use the notation ξ_i, η_i, u_i, v_i and q_i for $\xi_i^{(j)}$, $\eta_i^{(j)}$, $u_i^{(j)}$, $v_i^{(j)}$ and $q_i^{(j)}$. Thus, for a heton travelling along the x-axis at a constant velocity U, the stationarity condition in a boundary point $(\xi_i(\lambda), \eta_i(\lambda))$ of a PV patch located in layer i is

$$v_i(\xi_i, \eta_i)\dot{\xi}_i - [u_i(\xi_i, \eta_i) - U]\dot{\eta}_i = 0, \quad i = 1, 2, \tag{2.13}$$

where the velocity components u_i and v_i are determined by (2.6)–(2.11). So, in searching for a stationary heton, the task is to find a constant U and the functions $\xi_i(\lambda)$ and $\eta_i(\lambda)$ that satisfy (2.13) at any $0 \leqslant \lambda \leqslant \Lambda$ for $i = 1, 2$; of course, some parameters identifying the heton should be prescribed (see below). At this stage, for definiteness,

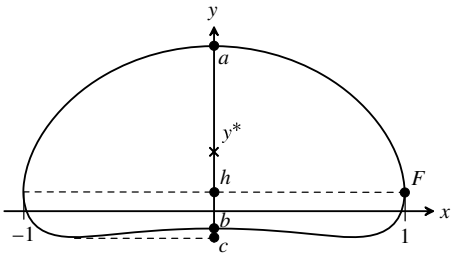

FIGURE 1. The upper-layer PV patch of a two-layer doubly symmetric heton. Here F is the front point with the coordinates $x = 1$ and $y = h$. The symbols a, b, c, h and y^* next to the marked points on the y-axis designate the ordinates of these points (see the text); the point $(0, y^*)$ marked by a cross is the patch centroid.

we assume that the positive PV patch resides in the upper layer ($q_1 = 1$ and $q_2 = -1$) and look for hetons with $U \geqslant 0$, i.e. those propagating rightward or standing in place (referred also to as static). Owing to the $y \to -y$ and $t \to -t$ symmetry of the f-plane model given by (2.1) and (2.2), a symmetry transformation about the x-axis of the solutions found will yield hetons propagating leftward.

The iterative procedure used here virtually repeats that described in our previous paper (Makarov & Kizner 2011) devoted to barotropic dipole equilibria. As in the barotropic case, the procedure allows the construction of translating and rotating relative equilibria; in particular, asymmetric translational hetons can be constructed, composed of patches that differ in PV, area and shape. Also symmetric about the x-axis but asymmetric about the y-axis hetons can be obtained. A solution of this kind, which we call 'dehiscent', appears as a couple of quasi-elliptic PV patches (with generally non-zero separation) whose principal axes make an angle which does not exceed 90°; such a solution requires suitable initialization of the iterative procedure. However, the subject of this paper is doubly symmetric hetons; we capture them with a version of the procedure which is akin to the mirror-symmetric version of the contour-dynamics algorithm (see § 2.2). Thus, the shape of only the upper-layer patch (figure 1) is sought, while the shape of the remaining patch is obtained as a mirror image of the first one. According to our computations, the symmetry of a heton about the y-axis is guaranteed if the iterative procedure is initialized by a contour, which is symmetric about this axis.

As will be seen below (§ 3.1), the doubly symmetric hetons obtained with our algorithm can be thought of as a two-parameter family. It would be only natural to consider the hetons as depending on γ, the heton's size relative to the Rossby radius, and the separation d between the centroids of the upper and lower PV patches normalized by the length scale L (defined in § 2.1 as the dimensional mean radius of heton's PV patch). However, practically, d is not always the best parameter to characterize the geometry of a dipole (e.g. Dritschel 1995; Makarov & Kizner 2011). Our computations (§§ 3.1 and 4) suggest that a more convenient parameter for this purpose can be the ordinate h of the front point F normalized by a new length scale L^*, the patch half-length in the x-direction (see figure 1). We compared this approach with an alternative algorithm, in which the input parameters for the construction of a heton solution were parameters γ and d. The comparison showed that the set of solutions obtained with the procedure based on h and L^* is wider than the set obtained

with the alternative (γ, d)-based algorithm, although, when the alternative procedure converges, the solutions obtained with the two methods are identical.

Once the distance from the x-axis to the front point F is normalized by the patch half-length, the same normalization suggests itself for any length parameter. Thus, we will be looking for doubly symmetric heton solutions as determined by a pair of parameters $\gamma^* = L^*/L_{Ro}$ and h. In this parameter space, all of the dipoles have the same non-dimensional length 2 (the distance from the rearmost point to the front point F), and the remaining geometrical parameters, in particular, the non-dimensional ordinate y^* of the centroid of the upper-layer patch and the patch area S, become functions of γ^* and h, i.e. $y^* = y^*(\gamma^*, h)$ and $S = S(\gamma^*, h)$. Clearly, as soon as a heton solution at a given pair of parameters γ^* and h is found, one can determine its y^* and S, and then calculate parameters γ and d as

$$\gamma = \gamma^* \sqrt{S(\gamma^*, h)/\pi}, \quad d = 2y^*(\gamma^*, h)/\sqrt{S(\gamma^*, h)/\pi}. \tag{2.14}$$

Note that the conditions $U \geqslant 0$ and $d \geqslant 0$ (or $y^* \geqslant 0$) are equivalent.

When constructing the heton solutions, in most of the computations, we use up to 500 nodes and stop the computations when both the relative distance between two successive approximations of the contour and the relative difference between two successive estimates of U, become less than a prescribed tolerance, $\varepsilon = 10^{-9}$ (for details, see Makarov & Kizner 2011). In some cases (say, near the point A on the (γ^*, h) plane, which will be discussed in § 3) we had to use 2500 nodes and the tolerance $\varepsilon = 10^{-14}$.

3. Heton equilibria

3.1. *Overview of the solutions found*

Doubly symmetric solutions were constructed with γ^* varying in the range $10^{-13} < \gamma^* \leqslant 10$ at a step 0.2, and h varying in the range $-0.34 \leqslant h \leqslant 1$ at a step 0.02; for computational reasons, the value $\gamma^* = 10^{-13}$ was used instead of $\gamma^* = 0$. Overall, over 2800 stationary solutions were constructed. In figure 2, some characteristics of translating hetons found are shown as contour lines on the (γ^*, h) plane. The shapes of a number of hetons overlaid with the isolines of the upper-layer comoving streamfunction, $\psi_1 + Uy$, are shown in figure 3.

As expected, doubly symmetric hetons exist for, apparently, any positive values of parameters γ^* and h (figures 2*a–c*, 3*a*). A result that is a little more surprising is the existence of solutions with negative h on the right of point A whose coordinates are $\gamma_A^* \approx 2.840$ and $h = 0$ (figures 2, 3*b*). To distinguish between the solutions with $h \geqslant 0$ and $h < 0$, we shall refer to them as to ordinary and cross-over hetons, respectively (because of the unusual shape of the latter).

For any γ^*, there is a minimal value of h allowing the existence of rightward or static doubly symmetric hetons. The borderline of the region, where such heton solutions exist, consists of two parts, a rectilinear piece OA, where $0 \leqslant \gamma^* \leqslant \gamma_A \approx 2.840$ and $h = 0$, and a curvilinear piece, where $\gamma^* > \gamma_A$ and $h < 0$. The shape of this curvilinear part (the bold solid line in figure 2) is estimated numerically as some nonlinear function $h = \Phi(\gamma^*) < 0$ of parameter γ^*. In a solution with a negative h, the centroid and the front point of a PV patch are located on opposite sides of the x-axis, so the two patches overlap in a somewhat exotic, cross-over manner (see the lowest row in figure 3*a* at $3 \geqslant \gamma^* \geqslant 5$ and figure 3*b*). Note that cross-over solutions have never been discussed in the literature before. Below (§ 4) we shall see that the cross-over hetons are all unstable.

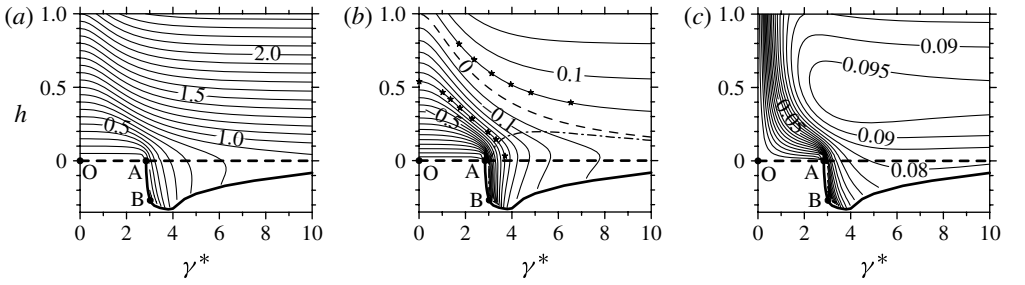

FIGURE 2. Isolines of selected characteristics of translating doubly symmetric hetons on the (γ^*, h) plane. (*a*) Relative separation d between the vorticity centroids (see the second of relationships (2.14)). (*b*) The ratio b/a, which at $b/a \leqslant 0$ can serve as a measure of the overlap of the upper and lower PV patches; the thin dashed line (at which $b/a = 0$) demarcates the overlapping and non-overlapping hetons; dash-dotted line, at which $c - b = 0$, indicates the upper bound of the region occupied with hetons composed of beanlike patches; asterisks represent Polvani's (1991) solutions (6 of the 12 solutions corresponding to $b/a = 0.05$ do not fit into the plot frame). (*c*) The heton translation speed U. In all of the panels, the region filled with isolines is the region where the rightward translating heton solutions can be constructed. The rectilinear segment OA of the bold dashed line (where $h = 0$) corresponds to static, circular purely baroclinic (thus static) hetons that are limiting to the translating hetons as $h \to \infty$ at $\gamma < \gamma_A$; the remainder of the bold dashed line (at $\gamma_A < \gamma$) represents static circular fully baroclinic solutions that exist along with the rightward-translating hetons whose front points lie on the x-axis. The bold solid line is the borderline of the region where hetons with $h < 0$ exist (the $h = \Phi(\gamma^*)$ line). The region between the bold dashed line and the bold solid line is occupied by the cross-over solutions, in which the centroid and the front point of a PV patch are located on opposite sides of the x-axis; static cross-over hetons correspond to the solid bold line segment AB.

The behaviour of parameters d and b/a is of particular interest, because Makarov & Kizner (2011) used the separation to identify barotropic dipoles, whereas Polvani (1991) employed parameter b/a to compute finite-core hetons. With this approach, however, Polvani did not obtain the cross-over solutions. At $h > 0$ and $\gamma^* < \gamma_A$, the separation d and the ratio b/a monotonically depend on h at any given γ^* (figure 2*a,b*). At $\gamma^* > \gamma_A$ and $\Phi(\gamma^*) \leqslant h < \infty$, the dependences of d and b/a on h are not monotonic; for example, at a fixed $\gamma^* > \gamma_A$, parameter b/a reaches its minimum at a positive h (figure 2*b*). This explains why the use of parameter h in constructing the family of stationary solutions is preferred over that of d or b/a.

The thin dashed line in figure 2(*b*) indicates the dipoles in which $b = 0$; below this line, b/a is negative. In the hetons occupying the region beneath the dash-dotted line, the patches are beanlike, according to Polvani's (1991) terminology (see e.g. figure 3, $h = -0.1, 0, 0.1$ and $\gamma^* = 4, 5$). Noticeably, the thin dashed line goes above the dash-dotted line. This means that we cannot expect that the overlap of the upper and lower patches can be present in the front and rear parts of a heton and, at the same time, be absent in its central part. Thus, in non-overlapping hetons, necessarily, $b/a \geqslant 0$. In overlapping hetons, i.e. where $b/a < 0$, this ratio can serve as a reasonable measure of the overlap. However, as figure 3 suggests, this measure is meaningful only in application to ordinary hetons (at $h \geqslant 0$). The overlap in ordinary hetons is most pronounced at $h = 0$ and $0 < \gamma^* \leqslant \gamma_A^*$, and it decreases as h increases and γ^* goes to the right of γ_A^* (figures 2*b* and 3*a*). When γ^* varies from 0 to approximately 1 and $0 < h \leqslant 1$, the translation speed depends monotonically on each of the arguments γ^*

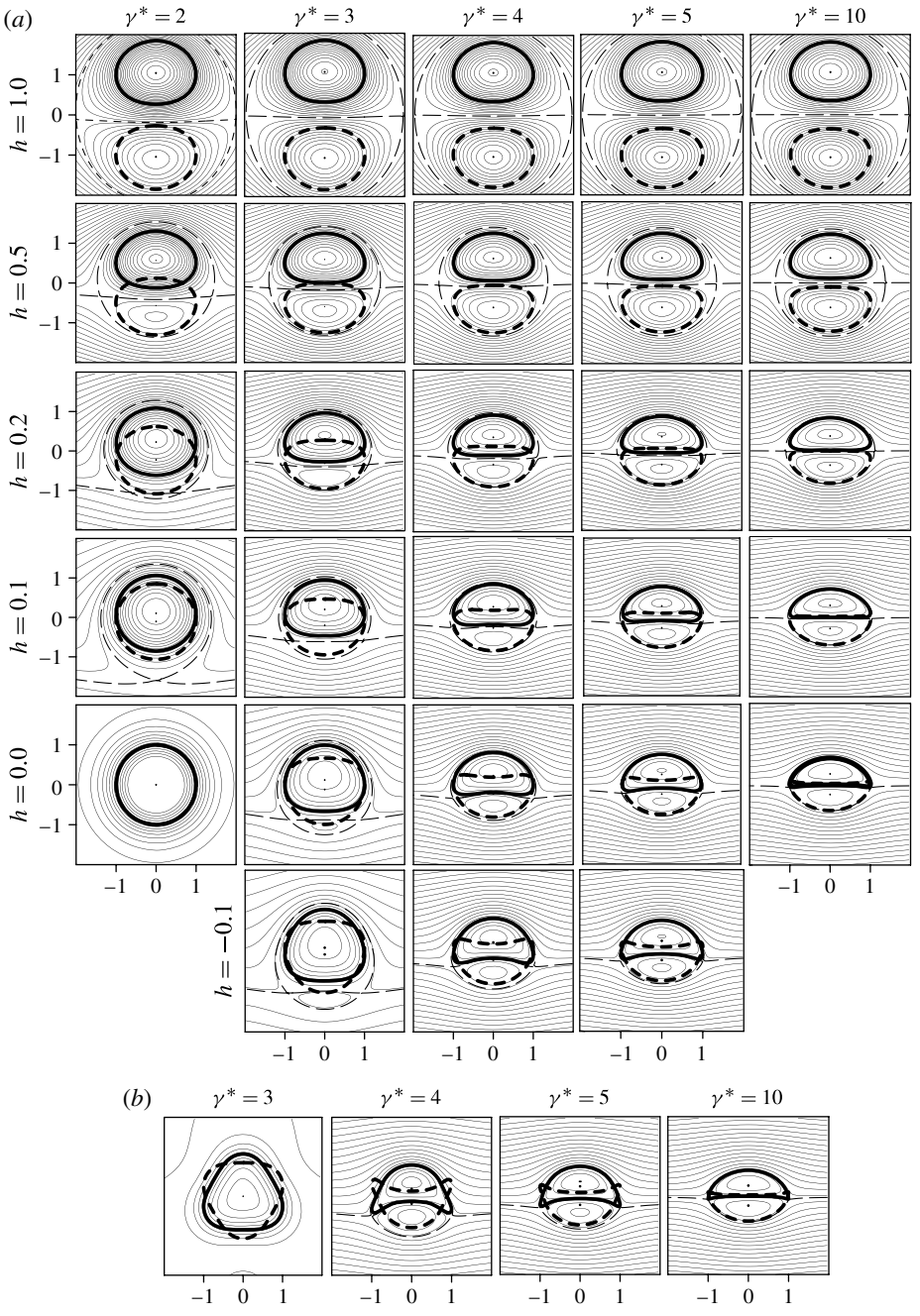

FIGURE 3. Examples of doubly symmetric heton solutions computed at different combinations of parameters γ^* and h (indicated on the top and left). (*a*) Hetons at $h \geqslant -0.1$. (*b*) Heton solutions near the boundary $h = \Phi(\gamma^*)$ of the region were the solutions exist (figure 2). Bold solid and dashed lines indicate the edges of the PV patches in the upper and lower layers, respectively; thin solid lines are the streamlines in the upper layer (given at a step 0.01); thin dashed lines are the separatrix streamlines in the upper layer; dots, centroids of the PV patches.

and h, but outside this region U becomes a two-valued function of h (at any given γ^*) reaching its maximum in the vicinity of the line $h = 0.5$ (figure 2*c*). This appears quite natural if we recall the dependence of the translation speed on the separation in point-vortex hetons (Hogg & Stommel 1985).

A well-known heton solution is given by a pair of circular PV patches of the same radius positioned one exactly above the other (Kozlov *et al.* (1986) term such a heton axially symmetric). Such trivial solutions correspond to $h = 0$ and exist at any γ^* (figure 2, bold dashed line). In a solution of this kind, $\psi_{BT} = 0$ identically, therefore its translation speed is necessarily zero (see, e.g. Kizner *et al.* 2002, 2003*a*,*b*), i.e. the heton is static. Numerically, a circular fully baroclinic solution with $h = 0$ is easily obtained in the range $0 < \gamma^* \leqslant \gamma_A^*$ (segment OA in figure 2); it is limiting to the translating solutions with the same γ^*. In contrast, at $\gamma^* > \gamma_A$ and $h = 0$, we managed to obtain static, fully baroclinic solutions only when the initial guesses were already close to circular; otherwise, the procedure converged to translating hetons with incomplete overlap of the patches (figure 3*a*, the panels in the row $h = 0$).

It is instructive to compare the hetons obtained by Polvani (1991) with ours. Polvani produces two tables with several parameters characterizing two series of solutions, namely 12 hetons at $b/a = 0.05$ and 8 hetons at $b/a = -0.3$, referred below to as series 1 and 2, respectively. Using some of these parameters, for each of the 20 Polvani's solutions we determine the relative separation d and, by setting d and γ (which differs from Polvani's γ by a factor $\sqrt{2}$), construct a heton solution via our alternative (γ, d) procedure (see § 2.3). Next, we calculate b/a and the translation speed U, as well as h and γ^* for our solutions, and compare our b/a and U with the b/a and the properly normalized translation speed of Polvani's hetons. For series 1, the discrepancy in b/a grows from 0.02 to 1 % with increasing γ, while the discrepancy in U remains approximately 0.05 % for the whole range of γ values. For series 2, with increasing γ, the discrepancy in b/a grows from 0.00 to 0.62 % as long as the PV patches remain convex, and for the only beanlike heton in this series, the discrepancy in b/a equals to 2.44 %; the discrepancy in U increases from 0.08 to 0.16 %. Owing to the pretty good agreement, we conclude that Polvani's (1991) solutions are members of the family of our doubly symmetric heton solutions (the 2 % discrepancy in a/b in the only beanlike heton is apparently due to the fact that this solution is close to the convergence bound of Polvani's algorithm, where the accuracy of his computations is the lowest). Because parameters h and g^* for our counterparts to Polvani's hetons are known, we can show these solutions in figure 2(*b*) (asterisks); in the figure caption, we loosely refer to them as to Polvani's hetons.

Classification of the doubly symmetric rightward translating and static hetons (i.e. with $d \geqslant 0$) on the (γ^*, h) and (γ, d) planes is summarized in figure 4. Comparison of figures 4(*a*) and 4(*b*) convinces us that the (γ^*, h) plane is indeed better suited for the construction and classification of the heton equilibria. For instance, on the (γ, d) plane (figure 4*b*), the boundaries of the region of existence of cross-over hetons intertwine due to the non-monotonic dependence of d upon h. On the other hand, the (γ, d) plane appears to be a more natural environment for the discussion of the heton stability (§ 4.1).

3.2. *Boundaries and limiting states*

In the limit of $\gamma^* \to 0$, (2.1)–(2.3) at $i = 1$ and $i = 2$ describe two independent two-dimensional flows. Thus, the two PV patches in a limiting heton do not interact and are circular, so the heton is static ($U = 0$) and the separation between the centres of the patches is $d = 2h$ (figure 2*a*,*c*). On the other hand, for any fixed γ^*, when

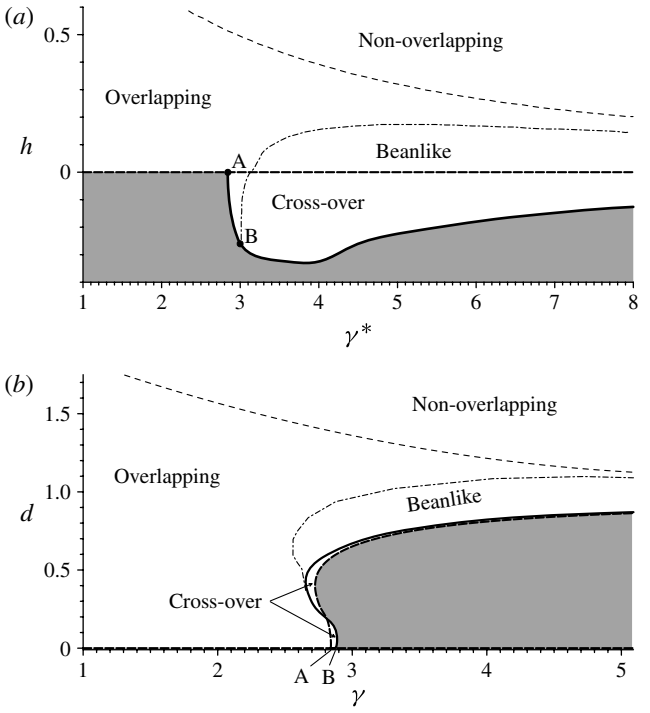

FIGURE 4. Classification of the doubly symmetric hetons with $d \geqslant 0$. (*a*) Regions in the (γ^*, h) plane occupied by solutions of different types. (*b*) Regions in the (γ, d) plane occupied by solutions of different types. In (*a,b*), thin dashed lines demarcate the regions of overlapping and non-overlapping hetons; beanlike hetons are found beneath or to the right of the dash-dotted lines; straight bold dashed lines represent static, purely baroclinic solutions; curved bold solid lines represent the solutions with $h = \Phi(\gamma^*)$; segment AB represents the static cross-over hetons. Shaded in (*a*) is the region on the (γ^*, h) plane, where no rightward translating hetons are found; its mapping on the (γ, d) plane is shaded in (*b*); curved bold dashed line in (*b*) represents translating hetons with $h = 0$. Translating cross-over solutions fill the region between the curved bold solid line and the straight dashed line in (*a*) and the two regions between the curved bold solid line and the curved bold dashed line in (*b*).

$h \to \infty$, the separation d goes to infinity and the barotropic interaction between the patches becomes the leading one. This is because at the periphery of a PV patch, as the distance from a PV patch increases, the barotropic flow induced by this patch dies out more slowly than the baroclinic flow. Therefore, in this limit too, the PV patches tend to become circles and $U \to 0$.

Another class of effectively barotropic limiting solutions is achieved as $\gamma^* \to \infty$. As (2.2) and (2.5) suggest, $\psi_{BC} \to 0$ in the limit of $\gamma \to \infty$ and, hence, as $\gamma^* \to \infty$. However, generally, ψ_{BT} does not vanish in this limit; so one may say that the flow in the two layers undergoes barotropization as $\gamma^* \to \infty$. In other words, although the two vorticity patches reside in different layers, the flows in the upper and lower layers tend to become identical as $\gamma^* \to \infty$. Accordingly, the PV patches constituting a heton tend to take the same shape as in the single-parameter family of barotropic uniform-vorticity dipoles first described by Pierrehumbert (1980); this fact was mentioned by Polvani (1991). In particular, at $h = 0$, the limiting shape to which the incompletely overlapped heton tends is the same as of the Sadovskii (1971) barotropic dipole

in which the boundaries of the patches have two vertices each and a common rectilinear boundary segment on the translation axis. (In contrast, the flow induced by a purely baroclinic circular heton solution mentioned in § 3.1 degenerates to zero with growing γ^*.) Obviously, the translation speed of the limiting two-layer heton with a 'barotropized' streamfunction is half that of a truly barotropic dipole of the same shape.

The line $h = \Phi(\gamma^*)$ bounding from below the region on the (γ^*, h) plane, in which cross-over heton equilibria exist (bold solid line in figures 2 and 4*a*), consists of two parts, the segment AB where the coordinates of point B are $\gamma_B^* \approx 3.022$ and $h_B \approx -0.269$, and a half-infinite segment where $\gamma^* > \gamma_B^*$. The hetons corresponding to the segment AB (as other cross-over hetons) are not fully overlapping. Thus, the barotropic flow associated with such a boundary solution is non-zero; yet these hetons do not move. This can happen only if $d = 0$, i.e. if the tendencies for self-propulsion generated by different parts of a cross-over heton extinguish each other. The shape of a heton of this kind resembles a star of David (figure 3*b*, $\gamma^* = 3$); it is composed of a pair of curvilinear convex Δ-like patches with a common centroid, around which the lower patch is turned by 180° relative to the upper one.

All of the boundary solutions with $\gamma^* > \gamma_B^*$ and $h = \Phi(\gamma^*)$ are translating since in these hetons $d \neq 0$. Here, in each layer, the edges of the PV patches coincide with the separatrices of the comoving streamfunction. The same feature is inherent in the two-layer counterpart of the Sadovskii dipole, to which our boundary solution apparently tends as $\gamma^* \to \infty$ (because, seemingly, $\Phi(\gamma^*) \to 0$ as $\gamma^* \to \infty$). The boundary solutions at $\gamma^* > \gamma_B^*$ cannot be achieved numerically, but we managed to approach them quite closely; in this way the shape of the line $h = \Phi(\gamma^*)$ was estimated. Examples of the boundary solutions are shown in figure 3(*b*).

3.3. *Bifurcations*

The common property of the solutions considered in §§ 3.1 and 3.2 is that $y^* \geqslant 0$, i.e. $d \geqslant 0$, so these hetons either travel rightward ($y^* > 0$) or are static, i.e. stand in place ($y^* = 0$). As mentioned in § 2.3, for each solution with $y^* > 0$, there exists a mirror-symmetric (about the x-axis) leftward-moving counterpart with $y^* < 0$. Thus, on the (γ^*, h)-plane, the line given by the pair of equations $h = -\Phi(\gamma^*)$ and $h = \Phi(\gamma^*)$ (bold line in figure 5*a*) bounds from above and below the region, in which any pair (γ^*, h) determines two solutions that differ not only in the direction of their translation, but also in the shape of the PV patches.

Most sharp gradients of the characteristics of heton equilibria are observed in the vicinity of the point A in which, as we saw, a family of static circular purely baroclinic solutions with $h = 0$ (represented by a dashed line in figures 2 and 5*a*) bifurcates from the translating hetons (namely, from those whose front points are on the x-axis). Another set of hetons that bifurcates from the translating solutions in point A is the family of cross-over hetons. Static cross-over solutions, a subclass of the family of cross-over solutions with $d = 0$, are represented in figure 5(*a*) by segment BAB′ of the solid line bounding the region where both rightward- and leftward-translating hetons exist; the point labelled B′ is symmetric to B about the line $h = 0$.

Contour lines of γ^* on the (h, U) plane (figure 5*b*) and of h on the (γ^*, U) plane (figure 5*c*) give additional information on bifurcations. On the (h, U) plane, all of the isolines of γ^* with $\gamma^* < \gamma_A^* \approx 2.840$ smoothly pass through the point with the coordinates $h = 0$ and $U = 0$. In contrast, the isolines with $\gamma > \gamma_A^*$ break when they run into the straight-line segment labelled BB′ in figure 5(*b*). Recall that, on the

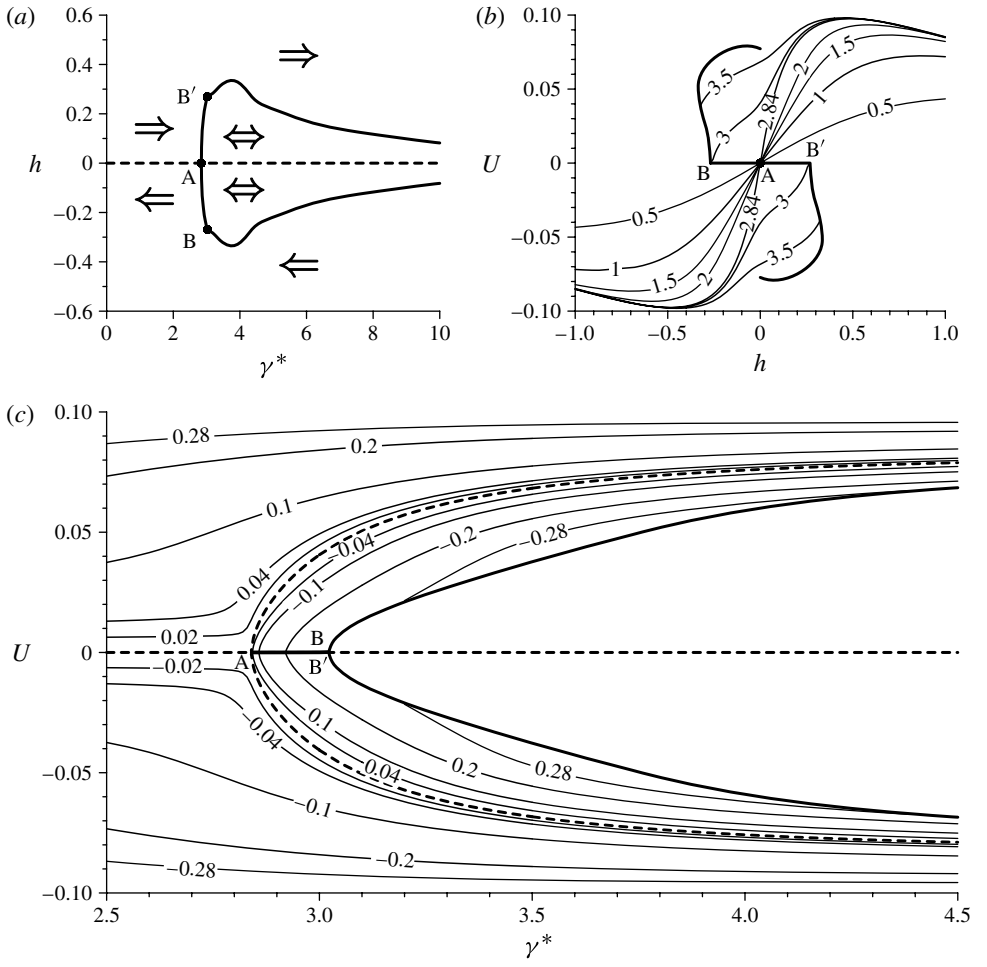

FIGURE 5. Bifurcations of heton equilibria. (*a*) Regions on the (γ^*, h) plane, where the hetons travelling rightwards or leftwards exist; arrows label the directions of the heton translation. Shown in bold is the line $h = \pm\Phi(\gamma^*)$ bounding the region on the (γ^*, h) plane where both rightward and leftward hetons exist (labelled by bidirectional arrows); points A and B are the same as in Figures 2 and 4, and B′ is symmetric to B about the γ^*-axis. (*b*) Contour lines of γ^* as a function of h and U (thin lines). (*c*) Contour lines of h as a function of γ^* and U (thin lines). In panels (*a*) and (*c*), dashed lines represent the hetons with $h = 0$ (some of them are static and others are not); in panels (*b*) and (*c*), symbols A, B and B′ label the same solutions as in (*a*). In all of the panels, the bold segments AB and AB′ represent the static cross-over hetons, and the remaining bold lines represent translating boundary cross-over hetons (but ordinary solutions are also present on the bold lines).

(γ^*, h) plane, the static cross-over solutions with negative and positive h correspond to the segments AB and AB′, respectively (see figures 2 and 4/5*a*). On the (γ^*, U) plane, however, these two kinds of solutions cannot be discriminated between because they fall into the same segment on the γ^*-axis (in figure 5*c*, the left end of this segment is labelled A, while the right end is deliberately labelled with two labels, B and B′). The isolines of h, which run into this segment, break off here. The isoline $h = 0$, when looked from left to right, splits in point A into three branches, upper, mid and lower,

at which the translation speed is positive, zero and negative, respectively. Note that, from point B (or B′) rightward on the γ^*-axis of the (γ^*, U)-plane, only axisymmetric fully baroclinic hetons exist (figure 5*c*).

4. Heton stability

4.1. *Determining the stability bounds*

We tested the stability of doubly symmetric hetons numerically based on contour-dynamics simulations with the above-described stationary solutions taken as initial states. In these tests, the numerical noise (coming from the discretization and round-off errors) served as permanently acting perturbations. Such perturbations are, generally, asymmetric. In the special case where the stability of doubly symmetric hetons to symmetric perturbations was studied, we employed the mirror-symmetric version of the algorithm (see § 2.2). In principle, even small local perturbations of the shape of the PV patches comprising a heton may affect the overall heton trajectory. However, as long as the variations in the heton shape remain small, such a response should not be interpreted as a manifestation of instability, since a relative equilibrium is considered.

Within the linear stability framework, instability of a vortical steady state to initial perturbations implies exponential growth with time of the perturbation magnitude. In contrast, in the nonlinear case, the growth of a perturbation can be limited even if the steady state is unstable. If, however, a small initial perturbation causes significant disruption of the shape of a vortical system and violates its structural integrity, one may speak of the structural instability (not to be confused with the structural instability with respect to changes in the parameters of a dynamical system). Although the numerical noise in a contour-dynamics simulation acts permanently, it affects the heton effectively in the same way as initial perturbations do, inducing a certain oscillation that in some circumstances may remain small (which is indicative of stability), but may grow in others (instability). In particular, the stability or instability of a heton can be judged by examining the variation in time of the perimeter of one of its PV patches, say, $P_1(t)$, the perimeter of the upper-layer vortex. We express this variation as the percentage relative to the initial perimeter, $\delta P(t) = 100[P_1(t)–P_1(0)]/P_1(0)$. This approach works reliably not only with symmetric perturbations, but with asymmetric perturbations as well, because, in response to slight asymmetric perturbations (asymmetric numerical noise), a heton which is close to the stability bound develops almost antiphase oscillations of the upper and lower patches. The oscillations persist as long as the heton retains its structural identity. Thus, the central question is how strong the oscillations are.

It is known that static fully baroclinic circular hetons ($h = d = 0$) are linearly stable if $\gamma < \gamma_{CR} \approx 1.705$, while at $\gamma > \gamma_{CR}$ the mode-2 perturbation becomes unstable, and its growth rate increases with increasing γ. This fact was established analytically (Kozlov *et al.* 1986; Flierl 1988; Helfrich & Send 1988). Therefore, in order to design a reasonably accurate procedure for the distinction between stable and unstable hetons, we start with the purely baroclinic circular hetons near the critical point $\gamma < \gamma_{CR} \approx 1.705$ and $d = 0$. As seen in figure 6(*a,b*), at $\gamma = 1.705$, parameter δP barely oscillates. The slow lowering (within 0.025 % by $t = 4000$) of the dashed curve corresponding to $\gamma = 1.705$ is due to a gradual shrinking of the patches typical of contour dynamics computations; the shrinking is so slight that the number of nodes at the contour bounding the PV patch remains unchanged by $t = 4000$. When we increase γ by 0.00025, thus entering into the zone of linear instability, δP demonstrates a weak oscillation whose amplitude is of the order of 0.05 and 0.075 % in the

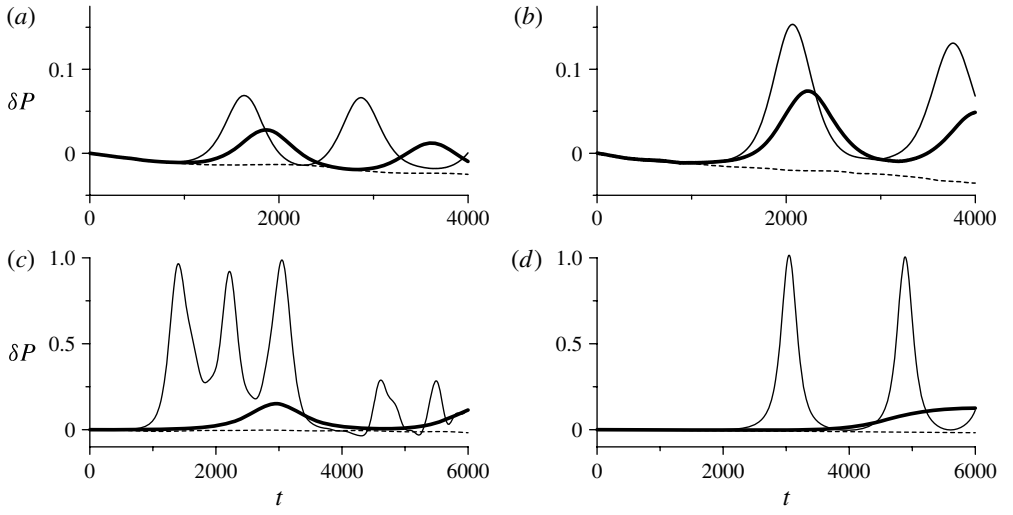

FIGURE 6. Determination of the stability bounds. Noise-induced oscillations of the perimeter of the upper-layer PV patch presented as the percentage relative variation $\delta P(t) = 100[P_1(t)–P_1(0)]/P_1(0)$. (*a*) Effect of asymmetric noise on the static circular hetons (i.e. with zero separation) at $\gamma = 1.705$ (dashed line), $\gamma = 1.70525$ (bold line) and $\gamma = 1.7055$ (thin solid line). (*b*) Same as in (*a*), but for symmetric noise. (*c*) Effect of asymmetric noise on the translating hetons with $d = 0.3$ at $\gamma = 1.794$ (dashed line), 1.79425 (bold line) and 1.7945 (thin solid line). (*d*) Effect of symmetric noise on the translating hetons with $d = 0.3$ at $\gamma = 1.804$ (dashed line), 1.80425 (bold line) and 1.8045 (thin solid line).

asymmetric and symmetric case, respectively. Taking one more 0.00025 step rightward, we obtain a stronger oscillation (the oscillations induced by the one- and two-step increase of γ are shown in figure 6*a,b* by bold and thin solid lines, respectively). The presence of a quasi-periodic regime at supercritical (in the sense of the linear stability) values of γ should not surprise us, since, in the simulations, we are dealing with nonlinear processes.

These preliminary computations suggest the following procedure for the high-resolution determination of the stability bounds. First, we make a rough estimate of the position of the stability bound on the (γ, d) plane and choose a reasonably thin domain enclosing the tentative bound. Then we fix d and, starting from a definitely stable solution within this domain, gradually increase γ with a step of 0.00025; alternatively, we can fix γ and decrease d with the same step (the choice of a proper version depends on the slope of the tentative bound). The process continues until the amplitude of the oscillations in δP reaches the level of 0.05 or 0.075 % in the asymmetric or symmetric case, respectively, or exceeds this level (bold solid lines in figure 6*c,d*). The subsequent increase of γ (decrease of d) leads to the growth in order of the magnitude of the amplitude (compare the positions of the bold and thin solid lines in figure 6). The penultimate value of γ (or d) in the above-described process is taken as the stability bound for the given d (or γ).

The shapes of the stability bounds on the (γ, d) plane shown in figure 7 are based on 42 points estimated in our stability tests as explicated above. For reasons of symmetry, in these diagram, only the region $d \geqslant 0$ is shown. The bounds of stability to asymmetric and symmetric perturbations are marked with diamonds and empty circles, respectively. In the interval from $\gamma = 1.705$ to $\gamma = 2.5$, the stability bounds are

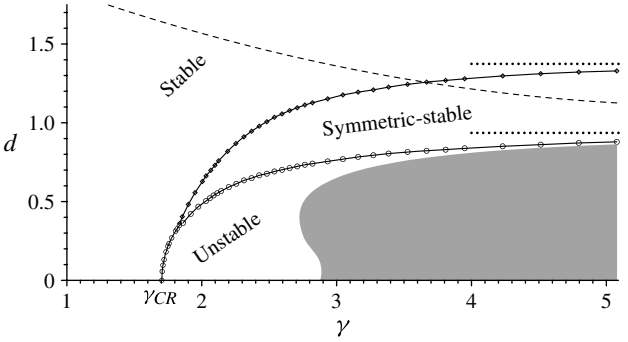

FIGURE 7. Stability bounds on the (γ, d) plane. Diamonds and empty circles mark the bounds of stability to asymmetric and symmetric perturbations, respectively. The region above the upper stability bound represents unconditionally stable hetons; the solutions belonging to the region between the two stability bounds are stable to symmetric perturbations and unstable to asymmetric perturbations; the region below the lower stability bound represents solutions unstable to the both types of perturbations. The asymptotic levels, to which the stability bounds approach as $\gamma \to \infty$, are given by dotted straight-line segments. Thin dashed line and shaded region, as in figure 4(*b*).

determined through varying the parameter γ, while at $\gamma > 2.5$, parameter d is varied. It might seem that, within the interval from $\gamma = 1.705$ to approximately $\gamma = 1.8$, the two bounds have a common segment. This is, however, just a graphical effect due to the thickness of the lines in figure 7.

Thus, we can conclude that the hetons comparable in size to the Rossby radius and smaller, i.e. at $\gamma < \gamma_{CR} \approx 1.705$, are stable in both senses. When the critical size γ_{CR} is exceeded, the heton stability becomes monotonically dependent on the separation, i.e. the larger the heton, the higher the separation required for the stability; and the separation needed for the stability to symmetric perturbations is smaller than that required for the stability to arbitrary perturbations (figure 7). These results are in qualitative agreement with the observations made earlier with two- and three-layer β-plane modons bearing smooth baroclinic riders (Kizner *et al.* 2002).

As $\gamma \to \infty$, i.e. when the flow in the two layers undergoes barotropization (see § 3.2), the two stability bounds approach two different asymptotic levels. In this limit, the stability properties of hetons must be the same as in barotropic dipoles. Indeed, the estimated asymptotic threshold separations for the stability to asymmetric (arbitrary) and to symmetric perturbations are quite close to $d \approx 1.374$ and $d \approx 0.936$, respectively (see figure 7, where these asymptotes are shown by dotted lines). The first of these bounds, $d \approx 1.374$, corresponds to Dritschel's (1995) estimate of the linear stability bound for barotropic dipoles, and the second bound, $d \approx 0.936$, is the separation between the centroids in the Sadovskii dipole, i.e. the minimum possible separation in barotropic dipoles which were all shown to be stable to symmetric perturbations (Makarov & Kizner 2011). Note that, due to the different choice of the length scale, the stability bounds provided here and in the work by Makarov & Kizner (2011) differ by a factor $\sqrt{\pi}$.

As indicated in figure 7, all non-overlapping hetons are stable to symmetric perturbations and, at $\gamma < 3.66$, they are stable to arbitrary perturbations as well. At $\gamma > 3.66$, there is a sector on the (γ, d) plane, where moderately separated non-overlapping hetons are unstable to arbitrary, asymmetric perturbations. For a non-

overlapping heton to be unstable, the separation d must necessarily be below the asymptotic stability bound, i.e. less than 1.374 (figure 7). Beanlike hetons are always unstable to asymmetric perturbations; however, at approximately $\gamma > 2.55$, beanlike solutions with a sufficient separation can be stable to symmetric perturbations (see figures 4*b* and 7). All cross-over hetons are unstable to perturbations of both types.

4.2. *Interrelation between instability and bifurcation*

The issues of bifurcations and behaviour of perturbed circular hetons, in our opinion, are interrelated. Therefore, we shall touch now very briefly upon the nonlinear evolution of perturbed purely baroclinic circular hetons in the supercritical region $\gamma > 1.705$ (a special study of the non-stationary regimes in perturbed stable and unstable hetons is now in preparation; it will be published elsewhere).

Kinematically, the oscillation of an initially circular baroclinic heton consists in synchronous periodical elongation of its PV patches (this behaviour was first observed by Helfrich & Send (1988)). In a similar way behave slightly perturbed hetons that are represented by the points (γ, d) adjacent to the 'common' segment of the stability bounds (figure 7) to the right of it. Remarkably, on the (γ, d) plane, along this part of the bound of stability to symmetric perturbations, the family of dehiscent solutions bifurcates from the doubly symmetric solutions. A dehiscent solution is obtained by initializing the iterative procedure by two separated ellipses whose principal axes make an angle of $\sim 20°$; such a solution possesses symmetry about the x-axis, but is asymmetric about the y-axis (§ 2.3). Bifurcations in dynamical systems are usually related to the emergence of instabilities. Therefore, the bifurcation of the dehiscent hetons serves as one more piece of evidence in favour of the correctness of our determination of the stability bounds for the doubly symmetric solutions.

The limiting value of γ, at which the increase in the oscillation amplitude does not affect the integrity of an initially circular purely baroclinic heton (i.e. does not lead to structural instability), is ~ 1.752. When the value 1.752 is overstepped, the elongation of the PV patches becomes accompanied by some cross-clamping, so the whole structure resembles in shape two crossed dumbbells. This process culminates in splitting the heton into two hetons that run in opposite directions (Helfrich & Send 1988; Sokolovskiy & Verron 2000). As our simulations suggest, the two emerged translating hetons are not steady, but oscillate around some stable steady states that can be depicted by one of our stationary solutions.

Continuing to increase gamma, we reach the next critical point, $\gamma \approx 2.840$, starting from which, mode 3 becomes unstable (Kozlov *et al.* 1986; Flierl 1988; Helfrich & Send 1988). In the second supercritical region, next to 2.840, the growth rate of mode 2 exceeds that of mode 3. Therefore, as before, a perturbed heton splits into two translating hetons. However, when gamma becomes larger than approximately 4.75, mode 3 begins to prevail, and a slightly perturbed heton takes the form of a pair of curvilinear Δ-like patches turned by some angle relative to each other, that is, becomes similar in shape to a static cross-over solution shown in figure 3(*b*) (leftmost panel). In this case, with the passage of time, three translating hetons detach from the parent structure (Helfrich & Send 1988; Sokolovskiy & Verron 2000). As established in § 3, the family of static cross-over solutions of the star-of-David kind bifurcates from the circular baroclinic hetons just at point A with the coordinates $\gamma_A^* \approx 2.840$ and $h = 0$ (figures 2 and 4*a*). On the (γ, d) plane, the coordinates of point A calculated via (2.14) are equal to those on the (γ^*, h) plane, i.e. $\gamma_A = \gamma_A^* \approx 2.840$ and $d_A = h_A = 0$. This is because the solution corresponding to point A is a circular purely baroclinic heton with a unit radius. Thus, the bifurcation occurs exactly at the second critical

point, where mode 3 becomes linearly unstable. In light of the theory of bifurcations in dynamical systems, such a coincidence is hardly accidental.

5. Conclusion

Aiming at the determination of the main parameters governing the stability of two-layer modons, we have considered a simplified model, namely, a two-parameter family of translating and static (i.e. standing in place) doubly symmetric finite-core heton equilibria. In terms of the potential vorticity, such a heton can be viewed as a pair of uniform PV patches, of which one (say, the positive PV patch) resides in the upper layer of a two-layer rotating fluid, and the other (the negative one) in the lower layer. The shapes of the patches are supposed to be symmetric about the translation axis and the transverse axis.

We obtained heton solutions numerically with an iterative procedure, which implements the condition that, in a frame of reference comoving with the heton, the bounding contours of the PV patches are stationary. The parameters identifying a doubly symmetric translating heton can be chosen in different ways. For instance, the mean radius γ of the PV patches (relative to the Rossby radius) and the non-dimensional horizontal separation d between their centroids (scaled with the mean radius) have a clear geometrical and physical meaning and are suitable for the discussion of the heton stability. However, at the stage of searching for the heton equilibria, this way of parameterization has some technical limitations. More convenient in this context appear the heton's half-length γ^* in the translation direction (again, relative to the Rossby radius) and the non-dimensional distance h from the front point of the upper-layer PV patch to the translation axis (scaled with the half-length). Following this path, we managed to obtain hetons in a wide range of shapes, including a novel class of solutions, the so-called cross-over hetons formed by overlapping beanlike PV patches whose centroids and front points are (generally) located on opposite sides of the translation axis. The barotropic flow associated with a cross-over solution is non-zero, because hetons of this type are not fully overlapping; yet among the cross-over solutions there is a subclass of static hetons, i.e. with $d = 0$. We examined the bifurcations of the solutions found, as well as the properties of the hetons in the limits of $\gamma^* \to 0$, $\gamma^* \to \infty$ and $h \to \infty$.

Stability of the heton equilibria was tested with fine-resolution contour-dynamics simulations, in which the permanently acting numerical noise served as a perturbing factor. Two kinds of stability were examined separately, the stability to arbitrary perturbations that do not preserve the symmetry of the initial state, and the stability to symmetric perturbations, which do not violate the initial symmetry. In addition, we discussed the interdependence between instability and bifurcations.

We found that the hetons comparable in size with the Rossby radius, and smaller ($\gamma < \gamma_{CR} \approx 1.705$), are stable in both senses. When the critical size γ_{CR} is exceeded, the heton stability becomes dependent on the separation; and the larger the heton, the higher the separation required for stability. The latter agrees with the numerical results of Kizner *et al.* (2002), who carried out just a few simulations with two- and three-layer β-plane modons bearing smooth baroclinic riders and considered the modon stability in terms of the degree of overlap. The β effect forces a modon to travel eastward and symmetrize about the translation axis to within an additive constant in the background PV field (Hesthaven, Lynov & Nycander 1993; Kizner *et al.* 2002, 2003*a*; Khvoles *et al.* 2007). Thus, there must be some similarity between the behaviour of the β-plane modons and f-plane hetons subjected to symmetric

perturbations (Kizner 2006, 2008). Indeed, we have found that non-overlapping and moderately overlapping hetons are stable to symmetric perturbations. Moreover, sufficiently separated non-overlapping hetons ($d > 1.374$) of any size are stable to arbitrary perturbations. Hetons whose separation is smaller than 1.374 can be unstable if they are constituted by large PV patches (with $\gamma > 3.66$). In the parameter plane (γ, d), such unstable hetons fill a relatively narrow sector above the region occupied by beanlike solutions. The characteristic feature of the beanlike hetons is the concave shape of their PV patches. Beanlike and cross-over hetons belong to the category of overlapping solutions. Beanlike hetons are unstable to asymmetric perturbations, but some of them can be stable to symmetric perturbations. The cross-over hetons, whose shapes are the most complex among all of the solutions found, are unstable in both senses.

The results presented above offer some new perspective in the investigation of the dynamics of two-layer modons. Now that the two-parameter family of doubly symmetric hetons is constructed and the stability bounds (with respect to symmetric and asymmetric disturbances) are known, a possibility arises to examine the presumably different oscillatory regimes and transitions typical of hetons moved off from equilibrium states determined by different pairs (γ, d). These issues will be addressed in a future study.

Acknowledgements

V.G.M. and M.A.S. are indebted to Bar-Ilan University for financial support and the hospitality extended to them during their work visits at BIU. V.G.M acknowledges the partial financial support of this research by the Mexican National Polytechnic Institute (SIP–IPN project 20110898) and the Mexican National Researchers System (SNI). The authors are grateful to the three anonymous referees for their helpful comments on the manuscript.

REFERENCES

CHAPLYGIN, S. A. 1903 One case of vortex motion in fluid. *Trans. Phys. Sect. Imperial Moscow Soc. Friends Nat. Sci.* **11** (2), 11–14 (English translation: Chaplygin, S. A. 2007 One case of vortex motion in fluid. *Regul. Chaotic. Dyn.* **12** (2), 102–114).

DEEM, G. S. & ZABUSKY, N. J. 1978 Vortex waves: stationary 'V-states', interactions, recurrence, and breaking. *Phys. Rev. Lett.* **40**, 859–862.

DRITSCHEL, D. G. 1988 Contour surgery – a topological reconnection scheme for extended integrations using contour dynamics. *J. Comput. Phys.* **77**, 240–266.

DRITSCHEL, D. G. 1989 Contour dynamics and contour surgery: numerical algorithms for extended, high-resolution modelling of vortex dynamics in two-dimensional, inviscid, incompressible flows. *Comput. Phys. Rep.* **10**, 77–146.

DRITSCHEL, D. G. 1995 A general theory for two-dimensional vortex interactions. *J. Fluid Mech.* **293**, 269–303.

FLIERL, G. R. 1988 On the stability of geostrophic vortices. *J. Fluid Mech.* **197**, 349–388.

FLIERL, G. R., LARICHEV, V. D., MCWILLIAMS, J. & REZNIK, G. M. 1980 The dynamics of baroclinic and barotropic solitary eddies. *Dyn. Atmos. Oceans* **5**, 1–41.

GRYANIK, G. R. 1983 Dynamics of singular geostrophic vortices in a two-layer model of the atmosphere (ocean). *Izv. Atmos. Ocean Phys.* **19**, 227–240.

HELFRICH, K. R. & SEND, U. 1988 Finite-amplitude evolution of two-layer geostrophic vortices. *J. Fluid Mech.* **197**, 331–348.

HESTHAVEN, J. S., LYNOV, J. P. & NYCANDER, J. 1993 Dynamics of nonstationary dipole vortices. *Phys. Fluids* A **5**, 622–629.

HOGG, N. G. & STOMMEL, H. M. 1985 The heton, an elementary interaction between discrete baroclinic geostrophic vortices, and its implications concerning eddy heat-flow. *Proc. R. Soc. Lond.* A **397**, 1–20.

KHVOLES, R., MCWILLIAMS, J. C. & KIZNER, Z. 2007 Non-coincidence of separatrices in two-layer modons. *Phys. Fluids* **19**, 056602.

KIZNER, Z. I. 1984 Rossby solitons with axisymmetrical baroclinic modes. *Dokl. USSR Acad. Sci.* **275**, 1495–1498.

KIZNER, Z. I. 1997 Solitary Rossby waves with baroclinic modes. *J. Mar. Res.* **55**, 671–685.

KIZNER, Z. 2006 Stability and transitions of hetonic quartets and baroclinic modons. *Phys. Fluids* **18** (5), 056601.

KIZNER, Z. 2008 Hetonic quartet: exploring the transitions in baroclinic modons. In *IUTAM Symposium on Hamiltonian Dynamics, Vortex Structures, Turbulence, IUTAM Bookseries* (ed. A. V. Borisov *et al.*), vol. 6, pp. 125–133. Springer.

KIZNER, Z. 2011 Stability of point-vortex multipoles revisited. *Phys. Fluids* **23**, 064104.

KIZNER, Z., BERSON, D. & KHVOLES, R. 2002 Baroclinic modon equilibria on the beta-plane: stability and transitions. *J. Fluid Mech.* **468**, 239–270.

KIZNER, Z., BERSON, D & KHVOLES, R. 2003*a* Non-circular baroclinic modons: constructing stationary solutions. *J. Fluid Mech.* **489**, 199–228.

KIZNER, Z., BERSON, D., REZNIK, G. & SUTYRIN, G. 2003*b* The theory of the beta-plane baroclinic topographic modons. *Geophys. Astrophys. Fluid Dyn.* **97**, 175–211.

KOZLOV, V. F., MAKAROV, V. G. & SOKOLOVSKIY, M. A. 1986 Numerical model of the baroclinic instability of axially symmetric eddies in two-layer ocean. *Izv. Atmos. Ocean. Phys.* **22**, 674–678.

LAMB, H. 1895 *Hydrodynamics*, 2nd edn. Cambridge, Cambridge University Press.

LARICHEV, V. D. & REZNIK, G. M. 1976 Two-dimensional solitary Rossby waves. *Dokl. Acad. Nauk USSR* **231**, 1077–1080.

MAKAROV, V. G. 1991 Computational algorithm of the contour dynamics method with changeable topology of domains under study. *Model. Mekh.* **5**, 83–95.

MAKAROV, V. G & KIZNER, Z. 2011 Stability and evolution of uniform-vorticity dipoles. *J. Fluid Mech.* **672**, 307–325.

PIERREHUMBERT, R. T. 1980 A family of steady, translating vortex pairs with distributed vorticity. *J. Fluid Mech.* **99**, 129–144.

POLVANI, L. M. 1991 Two-layer geostrophic vortex dynamics. Part 2. Alignment and two-layer V-states. *J. Fluid Mech.* **225**, 241–270.

POLVANI, L. M., ZABUSKY, N. J. & FLIERL, G. R. 1988 Applications of contour dynamics to two-layer quasi-geostrophic flows. *Fluid Dyn. Res.* **3**, 422–424.

REZNIK, G. M. & SUTYRIN, G. G. 2001 Baroclinic topographic modons. *J. Fluid Mech.* **431**, 121–142.

SADOVSKII, V. S. 1971 Vortex regions in a potential stream with a jump of Bernoulli's constant at the boundary. *Z. Angew. Math. Phys.: J. Appl. Maths Mech.* **35**, 773–779.

SOKOLOVSKIY, M. A. 1988 Numerical modelling of nonlinear instability for axisymmetric two-layer vortices. *Izv. Atmos. Ocean. Phys.* **24**, 536–542.

SOKOLOVSKIY, M. A. & VERRON, J. 2000 Finite-core hetons: stability and interactions. *J. Fluid Mech.* **423**, 127–154.

WU, H. M., OVERMAN, II, E. A. & ZABUSKY, N. J. 1984 Steady-state solutions of the Euler equations: rotating and translating V-states with limiting cases. I. Numerical algorithms and results. *J. Comput. Phys.* **53**, 42–71.

ZABUSKY, N. J., HUGHES, M. N. & ROBERTS, K. V. 1979 Contour dynamics for the Euler equations in two-dimensions. *J. Comput. Phys.* **30**, 96–106.